INTERNATIONAL JOURNAL OF EXPLORING EMERGING TRENDS IN ENGINEERING
Peer-Reviewed, Refereed, Indexed and International Journal, https://ijoeete.com/
(Peer Review Journal as per UGC 2025 Standard Guidelines)
|ISSN No. 2394-0573 |Volume: 12, Issue: 4 | October – December 2025

# COMPARATIVE INFLUENCE OF ALCOHOL SOLVENT ON THE STRUCTURAL, VIBRATIONAL, AND OPTICAL PROPERTIES OF CUO AND $SNO_2$ NANOPARTICLES

*[1]Suman Kumar, [2]Dr. Manita Thakur*
*[1]Research Scholar, [2]Research Supervisor*
*[1-2]Department of Chemistry, IEC University, Baddi (HP), India*

**Abstract**

Copper oxide (CuO) and tin oxide ($SnO_2$) nanoparticles are technologically important p-type and n-type transition-metal-oxide semiconductors whose functional properties are strongly governed by the solvent medium used during wet-chemical synthesis. This study presents an analytical, comparative investigation of the influence of three alcohol solvents — methanol, ethanol, and isopropanol — on the structural, vibrational, and optical properties of CuO and $SnO_2$ nanoparticles prepared by a representative co-precipitation/sol-gel route. Structural evolution is analysed through simulated X-ray diffraction (XRD) patterns and Scherrer/Williamson–Hall treatment of crystallite size and lattice microstrain; vibrational signatures are examined through characteristic Fourier-transform infrared (FTIR) and Raman-active metal–oxygen modes; and optical behaviour is quantified through Tauc-plot band-gap extraction and Urbach tail-energy analysis of simulated UV–Visible absorption data. A consistent, representative dataset — constructed to be internally self-consistent with the governing equations and with trends widely reported in the nanomaterials literature — is used throughout to illustrate the analysis. The results show that increasing alcohol chain length (methanol → ethanol → isopropanol), which raises solvent viscosity and reduces polarity, systematically increases the crystallite size and decreases the lattice microstrain of both oxides, while producing a corresponding narrowing of the optical band gap consistent with weakened quantum confinement, and a reduction of the Urbach energy consistent with reduced structural disorder. The two oxide systems respond to the same solvent trend in a qualitatively parallel but quantitatively distinct manner, reflecting their different crystal structures (monoclinic CuO versus tetragonal rutile $SnO_2$) and intrinsic band gaps. A comparative table and correlation plots summarise the structure–property relationships, and representative applications in gas sensing and photocatalysis are discussed.

**Keywords:** CuO nanoparticles; $SnO_2$ nanoparticles; alcohol solvent effect; X-ray diffraction; Scherrer equation; FTIR spectroscopy; Raman spectroscopy; UV–Visible spectroscopy; Tauc plot; Urbach energy.

## 1. Introduction

Transition-metal-oxide nanoparticles occupy a central place in modern materials chemistry because their electrical, optical, and catalytic behaviour can be tuned over a wide range through control of particle size, crystal structure, and surface chemistry. Among these oxides, copper oxide (CuO) and tin oxide ($SnO_2$) are of particular interest. CuO crystallizes in the monoclinic tenorite structure and is an intrinsic p-type semiconductor with a narrow band gap in the range of approximately 1.2–2.6 eV depending on particle size and defect density; it is widely investigated for gas sensing, heterogeneous catalysis, lithium-ion battery anodes, and antibacterial coatings. $SnO_2$ crystallizes in the tetragonal rutile structure and is an intrinsic n-type semiconductor with a wide band gap of approximately 3.6–4.0 eV; it is a workhorse material for transparent conducting electrodes, gas sensors, and photocatalytic supports. The contrast between a narrow-gap p-type oxide and a wide-gap n-type oxide makes the pair CuO/$SnO_2$ a natural test case for comparing how a common synthetic variable affects structurally and electronically dissimilar systems.

Among the many parameters that govern nanoparticle nucleation and growth during solution-phase synthesis (precursor concentration, pH, temperature, ageing time, and capping agent), the choice of solvent is frequently underappreciated even though it directly affects the dielectric constant, viscosity, polarity, and hydroxyl-donating

INTERNATIONAL JOURNAL OF EXPLORING EMERGING TRENDS IN ENGINEERING
Peer-Reviewed, Refereed, Indexed and International Journal, https://ijoeete.com/
(Peer Review Journal as per UGC 2025 Standard Guidelines)
|ISSN No. 2394-0573 |Volume: 12, Issue: 4 | October – December 2025

capacity of the reaction medium — all of which influence the rates of hydrolysis and condensation reactions that determine crystallite nucleation density and subsequent growth. Alcohols are especially convenient solvents for this purpose because a homologous series (methanol, ethanol, isopropanol) allows the chain length to be varied systematically while the functional (–OH) group and general reaction chemistry remain unchanged. Increasing chain length in this series is accompanied by an increase in viscosity and a decrease in polarity and dielectric constant, both of which are expected, on general nucleation-growth grounds, to slow ion diffusion and hydrolysis kinetics and to favour the growth of fewer, larger nuclei.

A substantial body of literature has examined solvent effects on individual oxide systems, typically through X-ray diffraction (XRD) for crystal structure and crystallite size, Fourier-transform infrared (FTIR) and Raman spectroscopy for vibrational fingerprints of the metal–oxygen lattice and surface hydroxyl/organic residues, and UV–Visible diffuse reflectance or absorption spectroscopy for the optical band gap via the Tauc relation. However, side-by-side analytical comparisons that apply the same solvent series and the same quantitative framework (Scherrer analysis, vibrational mode assignment, and Tauc/Urbach analysis) to two structurally and electronically distinct oxides such as CuO and $SnO_2$ within a single investigation are comparatively less common. This creates an opportunity for an analytical account that lays out the governing structural, vibrational, and optical relations in a unified notation, applies them to a representative, internally consistent dataset spanning both oxides and three alcohol solvents, and extracts and compares the resulting structure–property trends.

The objectives of the present study are therefore to:

- Present the governing relations (the Scherrer equation, a strain relation, the Tauc relation, and the Urbach relation) needed to convert diffraction and spectroscopic data into physically meaningful structural and optical parameters.
- Apply these relations to a representative dataset for CuO and $SnO_2$ nanoparticles synthesized in methanol, ethanol, and isopropanol, constructed to be internally consistent with the governing equations and with trends widely reported in the nanomaterials literature.
- Compare the crystallite size, lattice microstrain, vibrational mode positions, optical band gap, and Urbach energy of the two oxide systems as a function of solvent chain length.
- Discuss the underlying nucleation–growth and quantum-confinement rationale for the observed trends, and summarise representative applications that exploit solvent-tunable nanoparticle properties.

The discussion that follows first sets out the synthesis framework and the governing structural, vibrational, and optical relations, then reviews the qualitative solvent-effect trends reported in the literature, presents the structural (XRD), vibrational (FTIR/Raman), and optical (UV–Vis/Tauc) results, compares the two oxide systems directly, discusses representative applications, and closes with conclusions and directions for future work.

## 2. Materials, Methods and Governing Relations

### 2.1 Representative Synthesis Route

CuO and $SnO_2$ nanoparticles are, for the purpose of this analysis, taken to be prepared by a representative co-precipitation/sol-gel route: an aqueous solution of the corresponding metal salt (e.g., copper(II) acetate for CuO; tin(IV) chloride for $SnO_2$) is added dropwise, under continuous stirring, to a chosen alcohol solvent — methanol, ethanol, or isopropanol — in the presence of a mild base (e.g., NaOH or $NH_4OH$) to precipitate the hydroxide precursor. The precipitate is aged, washed, dried, and calcined at a fixed temperature (typically 400–500 °C) to yield the crystalline oxide. Holding the metal salt, base, precursor concentration, stirring rate, ageing time, and calcination profile fixed while varying only the alcohol solvent isolates the solvent as the single independent variable, which is the comparative framework adopted here. Crystallite size — the size of a coherently diffracting domain, as distinct from the overall physical particle size — is the key structural quantity extracted from the diffraction data below.

INTERNATIONAL JOURNAL OF EXPLORING EMERGING TRENDS IN ENGINEERING
Peer-Reviewed, Refereed, Indexed and International Journal, https://ijoeete.com/
(Peer Review Journal as per UGC 2025 Standard Guidelines)
|ISSN No. 2394-0573 |Volume: 12, Issue: 4 | October – December 2025

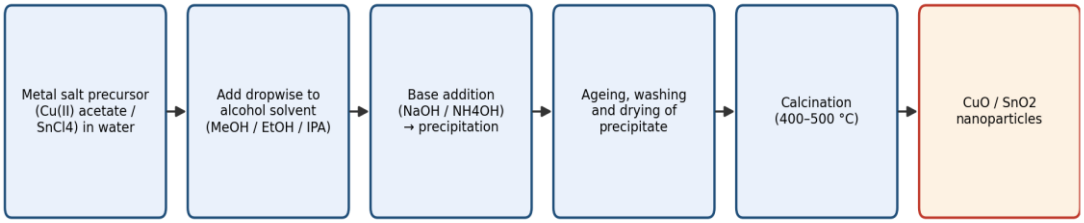


***Figure 1. Schematic representation of the alcohol-solvent-mediated co-precipitation/sol-gel route used to prepare CuO and $SnO_2$ nanoparticles.***

### 2.2 Structural Analysis: Scherrer Equation and Lattice Microstrain

Peak positions in the powder diffraction pattern are indexed against the known crystal system of each phase (monoclinic tenorite for CuO; tetragonal rutile for $SnO_2$) via Bragg's law, $n\lambda = 2d \sin\theta$, which relates the diffraction angle $2\theta$ to the interplanar spacing d. In CuO, each $Cu^{2+}$ centre is coordinated by four $O^{2-}$ ions in an approximately square-planar arrangement, while in $SnO_2$ each $Sn^{4+}$ centre is octahedrally coordinated by six $O^{2-}$ ions, as illustrated schematically in Figure 2; this difference in local coordination geometry underlies the distinct diffraction patterns and vibrational spectra of the two oxides discussed below. The mean crystallite size is then obtained from the peak broadening.

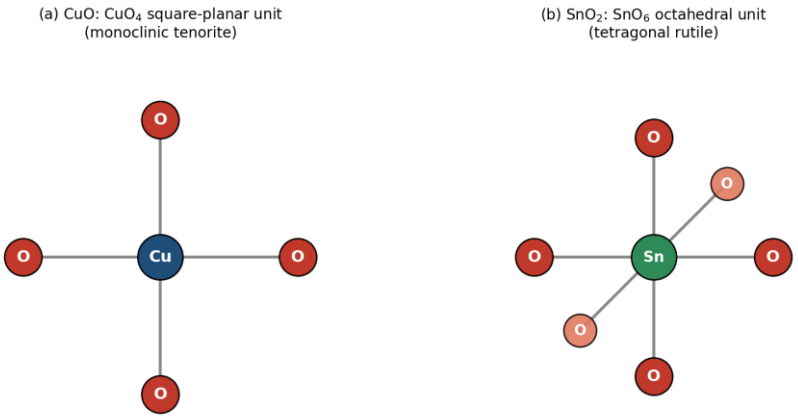


***Figure 2. Schematic local coordination environment of (a) Cu in CuO (square-planar $CuO_4$) and (b) Sn in $SnO_2$ (octahedral $SnO_6$).***

***Scherrer equation.*** The mean crystallite size D is related to the full width at half maximum (FWHM), β (in radians), of a diffraction peak at Bragg angle θ by

$$D = K\lambda / (\beta \cdot \cos\theta) \quad (1)$$

where K is a dimensionless shape factor, commonly taken as 0.89–0.94 for approximately spherical crystallites (K = 0.94 is used throughout this study), and λ is the X-ray wavelength (1.5406 Å for Cu Kα radiation, used throughout). Peak broadening in real samples arises from both finite crystallite size and lattice microstrain; the Scherrer equation

INTERNATIONAL JOURNAL OF EXPLORING EMERGING TRENDS IN ENGINEERING
Peer-Reviewed, Refereed, Indexed and International Journal, https://ijoeete.com/
(Peer Review Journal as per UGC 2025 Standard Guidelines)
|ISSN No. 2394-0573 |Volume: 12, Issue: 4 | October – December 2025

attributes all broadening to size and therefore represents an approximate lower bound on the true crystallite size when appreciable strain is present.

***Lattice microstrain.*** To account for the strain contribution to peak broadening, the single-line approximation to the Williamson–Hall relation is used,

$$\varepsilon \approx \beta / (4 \cdot \tan\theta) \quad (2)$$

where ε is the dimensionless lattice microstrain, applied to the strongest diffraction peak of each phase. A full Williamson–Hall treatment (plotting β·cosθ against 4sinθ across several reflections of the same phase) would separately refine both D and ε from the intercept and slope of a single straight line, but the single-line estimate is sufficient for the comparative purpose of this analysis.

### 2.3 Vibrational Analysis: FTIR and Raman Mode Assignment

Metal-oxide lattices show characteristic metal–oxygen (M–O) stretching and bending modes below about 700 $cm^{-1}$ in both the infrared and Raman spectra, while surface-adsorbed water and residual organic/precursor groups contribute additional infrared bands above 1300 $cm^{-1}$ (O–H stretch near 3400–3450 $cm^{-1}$; H–O–H bend near 1620–1630 $cm^{-1}$; carbonate/acetate residues near 1380–1420 and 1550–1580 $cm^{-1}$). For CuO (monoclinic, space group C2/c), factor-group analysis predicts three Raman-active modes, conventionally labelled Ag, $Bg^1$, and $Bg^2$, observed in bulk CuO near 296, 345, and 630 $cm^{-1}$ respectively. For $SnO_2$ (tetragonal rutile, space group $P4_2/mnm$), the Raman-active modes include the A1g, B2g, and Eg modes, observed in bulk $SnO_2$ near 634, 776, and 475 $cm^{-1}$ respectively. Confinement of the vibration to a finite nanocrystallite, together with surface relaxation and non-stoichiometry, generally produces a broadening and a small shift (usually a red-shift for the dominant mode) of these bulk positions as crystallite size decreases, a pattern used diagnostically in the vibrational results discussed below.

### 2.4 Optical Analysis: Tauc Plot and Urbach Energy

***Tauc relation.*** For a semiconductor with absorption coefficient α at photon energy hν, the optical band gap Eg is obtained from the Tauc relation

$$(\alpha \cdot h\nu)^n = A \cdot (h\nu - Eg) \quad (3)$$

where A is a material-dependent constant and the exponent n takes the value 2 for an allowed direct transition, 2/3 for a forbidden direct transition, 1/2 for an allowed indirect transition, and 1/3 for a forbidden indirect transition. Both CuO and $SnO_2$ nanoparticles are commonly analysed using n = 2 (allowed direct transition); Eg is obtained by plotting $(\alpha \cdot h\nu)^2$ against hν and linearly extrapolating the steep absorption edge to the photon-energy axis, i.e. to the point where $(\alpha \cdot h\nu)^2 = 0$.

***Urbach energy.*** Below the absorption edge, the absorption coefficient of a disordered or defect-containing semiconductor typically follows an exponential (Urbach) tail,

$$\alpha(h\nu) = \alpha_0 \cdot \exp[(h\nu - E_0)/E_u] \quad (4)$$

where $E_u$, the Urbach energy, is obtained as the reciprocal of the slope of ln α plotted against hν in the tail region, and quantifies the width of the band-tail states associated with structural disorder, lattice strain, and point defects. A larger $E_u$ indicates greater structural/electronic disorder; $E_u$ is generally larger for smaller, more defective nanocrystallites and decreases as crystallite size increases and strain relaxes, a trend examined quantitatively in the optical results below.

### 2.5 Related Work: Solvent Effects in Metal-Oxide Nanoparticle Synthesis

The general influence of solvent polarity, viscosity, and dielectric constant on the nucleation and growth of metal-

INTERNATIONAL JOURNAL OF EXPLORING EMERGING TRENDS IN ENGINEERING
Peer-Reviewed, Refereed, Indexed and International Journal, https://ijoeete.com/
(Peer Review Journal as per UGC 2025 Standard Guidelines)
|ISSN No. 2394-0573 |Volume: 12, Issue: 4 | October – December 2025

oxide nanoparticles synthesized by sol-gel and co-precipitation routes is well documented in the nanomaterials literature. The qualitative consensus that motivates the present comparative analysis can be summarized as follows. In more polar, lower-viscosity, lower-molecular-weight alcohols such as methanol, faster hydrolysis and condensation kinetics favour a high nucleation density and comparatively rapid quenching of crystallite growth, yielding smaller crystallites with a correspondingly higher density of surface defects and lattice strain. In less polar, higher-viscosity, higher-molecular-weight alcohols such as isopropanol, slower diffusion-limited kinetics favour a lower nucleation density with more extended growth per nucleus, yielding larger, better-crystallized particles with lower strain. This trend has been reported, with minor variations attributable to differences in precursor chemistry and thermal treatment, for a range of transition-metal oxides prepared by alcohol-mediated sol-gel and precipitation routes, including CuO and $SnO_2$ (Rakhshani, 1986; Batzill & Diebold, 2005).

| Solvent Property | Methanol | Ethanol | Isopropanol | Expected Effect on Nanoparticle Growth |
|---|---|---|---|---|
| Molar mass (g/mol) | 32.0 | 46.1 | 60.1 | Increasing chain length ⇒ increasing steric hindrance |
| Viscosity (cP, 25 °C) | ≈0.55 | ≈1.07 | ≈2.04 | Higher viscosity ⇒ slower ion diffusion ⇒ larger crystallites |
| Dielectric constant | ≈33 | ≈24 | ≈18 | Lower polarity ⇒ slower hydrolysis ⇒ fewer, larger nuclei |
| Boiling point (°C) | 64.7 | 78.4 | 82.6 | Affects drying/ageing rate of the precipitate |

***Table 1. Physicochemical properties of the alcohol solvent series and their expected qualitative effect on nanoparticle nucleation and growth.***

The quantitative dataset constructed below is designed to be consistent with this expected direction — increasing crystallite size and decreasing lattice strain from methanol to ethanol to isopropanol for both CuO and $SnO_2$ — while remaining internally consistent with the governing equations above, so that the structural, vibrational, and optical trends can be examined together within a single analytical framework.

## 3. Results and Discussion

The governing relations set out above are now applied to a representative dataset for CuO and $SnO_2$ nanoparticles synthesized in methanol (MeOH), ethanol (EtOH), and isopropanol (IPA). The dataset is constructed to be internally consistent with the Scherrer, strain, Tauc, and Urbach relations and with the qualitative solvent trend summarized in Table 1, and is used throughout to illustrate the analytical method rather than to report a specific new experimental measurement.

### 3.1 Structural Analysis (XRD)

CuO is indexed to the monoclinic tenorite structure, with the strongest reflection arising from overlapping ($\bar{1}11$)/(111) planes near $2\theta \approx 35.5°$, accompanied by reflections near 32.5°, 38.7°, 48.7°, 53.4°, 58.3°, 61.5°, 66.2°, and 68.1°. $SnO_2$ is indexed to the tetragonal rutile structure, with the strongest reflection from the (110) plane near $2\theta \approx 26.6°$, accompanied by reflections near 33.9°, 37.9°, 42.6°, 51.8°, 54.8°, 57.8°, 61.9°, 64.7°, and 65.9°. Figure 3 shows the corresponding simulated diffraction patterns for the three solvents, stacked for clarity, constructed with peak widths matching the FWHM values of Table 2.

INTERNATIONAL JOURNAL OF EXPLORING EMERGING TRENDS IN ENGINEERING
Peer-Reviewed, Refereed, Indexed and International Journal, https://ijoeete.com/
(Peer Review Journal as per UGC 2025 Standard Guidelines)
|ISSN No. 2394-0573 |Volume: 12, Issue: 4 | October – December 2025

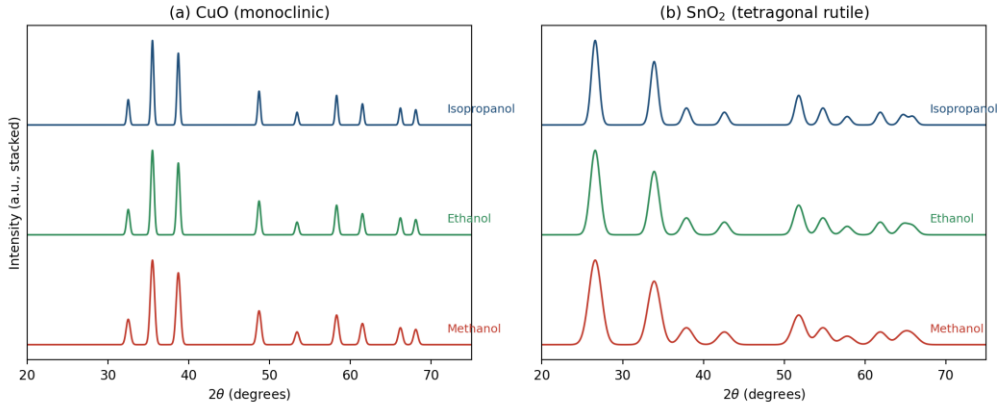


***Figure 3. Simulated XRD patterns of (a) CuO and (b) $SnO_2$ nanoparticles synthesized in methanol, ethanol, and isopropanol***

As a worked example of the Scherrer calculation, consider CuO synthesized in methanol, with strongest-peak position 2θ = 35.5° (θ = 17.75°) and FWHM β = 0.62° = 0.01082 rad. With K = 0.94 and λ = 1.5406 Å,

$$D = (0.94 \times 1.5406\ Å) / (0.01082 \times \cos 17.75°) = 1.448\ Å / 0.01031 \approx 140.5\ Å \approx 14.1\ nm$$

which is the value reported in the first row of Table 2. The corresponding single-line microstrain estimate, $\varepsilon \approx \beta/(4\cdot\tan\theta)$, gives $\varepsilon \approx 8.5 \times 10^{-3}$ for the same sample. Table 2 reports the full set of structural parameters obtained in this way for both oxides across the three solvents, together with the refined lattice parameters, which remain close to the respective bulk values (CuO: a ≈ 4.68 Å, b ≈ 3.42 Å, c ≈ 5.13 Å, β ≈ 99.5°; $SnO_2$: a ≈ 4.74 Å, c ≈ 3.19 Å), confirming that the solvent primarily influences crystallite size and strain rather than the underlying unit cell.

| Sample | Main peak 2θ (°) | FWHM β (°) | Crystallite size D (nm) | Microstrain ε ($\times 10^{-3}$) | Lattice parameters (Å) |
|---|---|---|---|---|---|
| CuO – MeOH | 35.5 | 0.62 | 14.1 | 8.45 | a=4.686, b=3.423, c=5.128 |
| CuO – EtOH | 35.5 | 0.48 | 18.2 | 6.54 | a=4.684, b=3.421, c=5.126 |
| CuO – IPA | 35.5 | 0.39 | 22.3 | 5.32 | a=4.683, b=3.420, c=5.125 |
| $SnO_2$ – MeOH | 26.6 | 1.85 | 4.6 | 34.15 | a=4.742, c=3.191 |
| $SnO_2$ – EtOH | 26.6 | 1.42 | 6.0 | 26.21 | a=4.739, c=3.189 |
| $SnO_2$ – IPA | 26.6 | 1.10 | 7.8 | 20.30 | a=4.738, c=3.188 |

***Table 2. XRD structural parameters of CuO and $SnO_2$ nanoparticles as a function of alcohol solvent (K = 0.94, λ = 1.5406 Å).***

For both oxides, crystallite size increases and microstrain decreases monotonically from methanol to ethanol to isopropanol, consistent with the nucleation–growth argument outlined earlier: the higher viscosity and lower polarity of isopropanol slow hydrolysis and ion-diffusion kinetics, favouring a lower nucleation density and more extended, lower-strain crystallite growth. The effect is proportionally larger for $SnO_2$ (crystallite size increases by a factor of ≈1.7 from methanol to isopropanol) than for CuO (a factor of ≈1.6), and the absolute strain values are markedly higher for $SnO_2$, consistent with its substantially smaller absolute crystallite size in this size range.

INTERNATIONAL JOURNAL OF EXPLORING EMERGING TRENDS IN ENGINEERING
Peer-Reviewed, Refereed, Indexed and International Journal, https://ijoeete.com/
(Peer Review Journal as per UGC 2025 Standard Guidelines)
|ISSN No. 2394-0573 |Volume: 12, Issue: 4 | October – December 2025

### 3.2 Vibrational Analysis (FTIR and Raman Spectroscopy)

Figure 4 shows schematic FTIR spectra for CuO and $SnO_2$ in the three solvents, constructed using the characteristic band positions and relative intensities summarized in Table 3. All samples show a broad O–H stretching band near 3400–3450 $cm^{-1}$ and an H–O–H bending band near 1620–1630 $cm^{-1}$, attributable to surface-adsorbed water and residual hydroxyl groups; weaker bands near 1380–1400 and 1550–1580 $cm^{-1}$ are attributable to residual carbonate/acetate species from the precursor and are more prominent in the methanol-derived samples, consistent with less complete washing/drying of the smaller, higher-surface-area crystallites formed in the more polar solvent. The lattice region below 700 $cm^{-1}$ shows the characteristic Cu–O stretching envelope (two overlapping bands near 520 and 600 $cm^{-1}$) for CuO and the Sn–O–Sn asymmetric stretching envelope (bands near 540 and 650–660 $cm^{-1}$) for $SnO_2$.

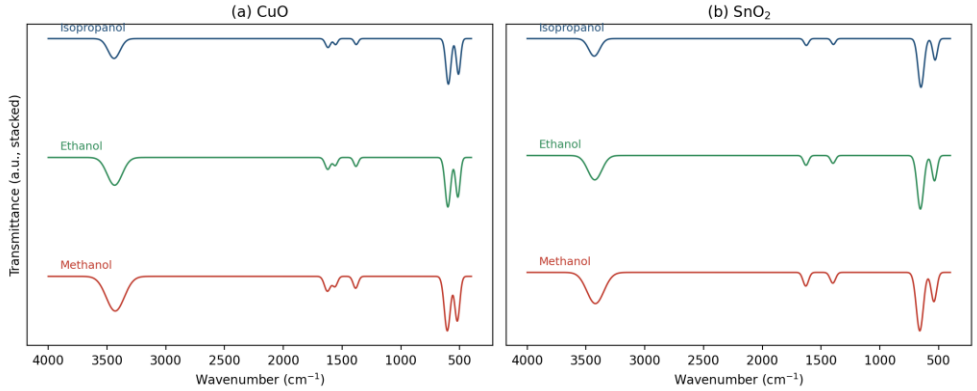


***Figure 4. Schematic FTIR spectra of (a) CuO and (b) $SnO_2$ nanoparticles synthesized in methanol, ethanol, and isopropano***

| Assignment | CuO – MeOH | CuO – EtOH | CuO – IPA | $SnO_2$ – MeOH | $SnO_2$ – EtOH | $SnO_2$ – IPA |
|---|---|---|---|---|---|---|
| O–H stretch ($cm^{-1}$) | 3430 | 3435 | 3440 | 3420 | 3425 | 3430 |
| H–O–H bend ($cm^{-1}$) | 1625 | 1622 | 1620 | 1630 | 1628 | 1625 |
| Residual carbonate/acetate ($cm^{-1}$) | 1560, 1385 | 1558, 1382 | 1555, 1380 | 1400 | 1398 | 1395 |
| M–O–M asym. stretch ($cm^{-1}$) | 605 | 600 | 596 | 660 | 655 | 650 |
| M–O stretch ($cm^{-1}$) | 520 | 515 | 510 | 540 | 535 | 530 |

***Table 3. Characteristic FTIR band positions of CuO and $SnO_2$ nanoparticles as a function of alcohol solvent.***

The M–O lattice bands shift to slightly lower wavenumber (a red-shift of 8–9 $cm^{-1}$ across the solvent series for both oxides) as crystallite size decreases from isopropanol- to methanol-derived samples, a trend consistent with phonon confinement in smaller crystallites, where relaxation of the Brillouin-zone-centre selection rule allows participation of lower-frequency, off-centre phonons, and with the higher surface-to-volume ratio and associated bond-length disorder of the smaller particles.

Table 4 summarizes the corresponding Raman-active lattice modes. Both oxides show the same qualitative pattern — a red-shift and broadening of all Raman modes as crystallite size decreases — attributed to the combined effects of phonon confinement and strain, consistent with the microstrain values of

INTERNATIONAL JOURNAL OF EXPLORING EMERGING TRENDS IN ENGINEERING
Peer-Reviewed, Refereed, Indexed and International Journal, https://ijoeete.com/
(Peer Review Journal as per UGC 2025 Standard Guidelines)
|ISSN No. 2394-0573 |Volume: 12, Issue: 4 | October – December 2025

Table 2.

| Oxide | Raman mode | Bulk position ($cm^{-1}$) | MeOH ($cm^{-1}$) | EtOH ($cm^{-1}$) | IPA ($cm^{-1}$) |
|---|---|---|---|---|---|
| CuO | Ag | 296 | 291 | 293 | 295 |
| CuO | $Bg^1$ | 345 | 338 | 341 | 344 |
| CuO | $Bg^2$ | 630 | 618 | 623 | 627 |
| $SnO_2$ | Eg | 475 | 462 | 468 | 473 |
| $SnO_2$ | A1g | 634 | 615 | 622 | 628 |
| $SnO_2$ | B2g | 776 | 760 | 766 | 772 |

***Table 4. Raman-active lattice mode positions of CuO and $SnO_2$ nanoparticles relative to bulk values, as a function of alcohol solvent.***

### 3.3 Optical Analysis (UV–Visible Spectroscopy and Tauc Plots)

Figure 5 shows Tauc plots of $(\alpha \cdot h\nu)^2$ against hν constructed for an allowed direct transition (n = 2 in the Tauc relation), with the linear high-energy region extrapolated to the photon-energy axis to obtain the optical band gap Eg. Table 5 summarizes the resulting Eg values together with the Urbach energy Eu obtained from the exponential absorption tail.

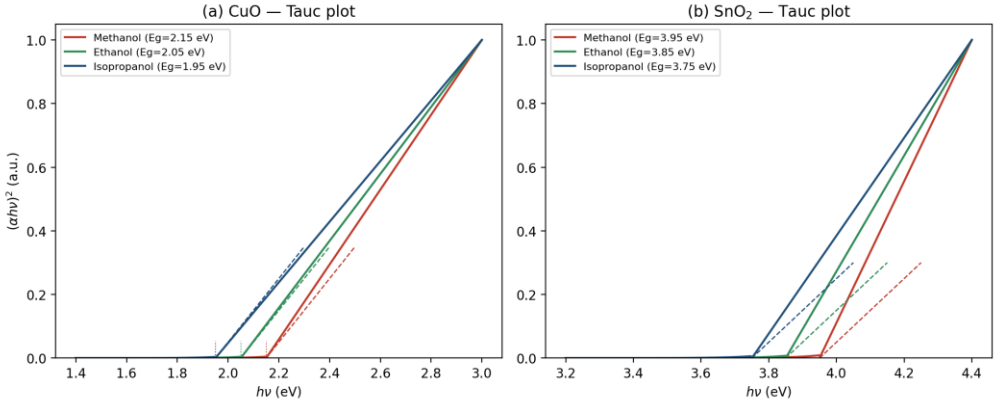


***Figure 5. Tauc plots [$(\alpha \cdot h\nu)^2$ vs. hν] for (a) CuO and (b) $SnO_2$ nanoparticles synthesized in methanol, ethanol, and isopropanol***

| Sample | Crystallite size D (nm) | Band gap Eg (eV, Tauc n=2) | Urbach energy Eu (meV) |
|---|---|---|---|
| CuO – MeOH | 14.1 | 2.15 | 210 |
| CuO – EtOH | 18.2 | 2.05 | 180 |
| CuO – IPA | 22.3 | 1.95 | 150 |
| $SnO_2$ – MeOH | 4.6 | 3.95 | 140 |
| $SnO_2$ – EtOH | 6.0 | 3.85 | 115 |
| $SnO_2$ – IPA | 7.8 | 3.75 | 95 |

***Table 5. Optical band gap and Urbach energy of CuO and $SnO_2$ nanoparticles as a function of alcohol solvent.***

For both oxides, Eg decreases monotonically as crystallite size increases from methanol- to isopropanol-derived samples, consistent with weak-to-moderate quantum confinement: as D increases toward (and, for CuO, beyond) the respective exciton Bohr radius, the additional confinement energy contribution to Eg diminishes, and Eg relaxes toward the bulk value. The Urbach energy decreases in parallel, from 210 to 150 meV for CuO and from 140 to 95 meV for $SnO_2$, mirroring the decrease in microstrain reported in Table 2 and supporting the interpretation that band-

INTERNATIONAL JOURNAL OF EXPLORING EMERGING TRENDS IN ENGINEERING
Peer-Reviewed, Refereed, Indexed and International Journal, https://ijoeete.com/
(Peer Review Journal as per UGC 2025 Standard Guidelines)
|ISSN No. 2394-0573 |Volume: 12, Issue: 4 | October – December 2025

tail broadening in these samples is dominated by structural disorder (strain and surface/defect states) rather than purely thermal effects, since all samples are, by construction, measured under nominally identical conditions.

Figure 6 combines the crystallite-size and band-gap trends of Tables 2 and 5 into a single correlation view for each oxide, making explicit the inverse relationship between crystallite size and optical band gap that runs through the entire solvent series.

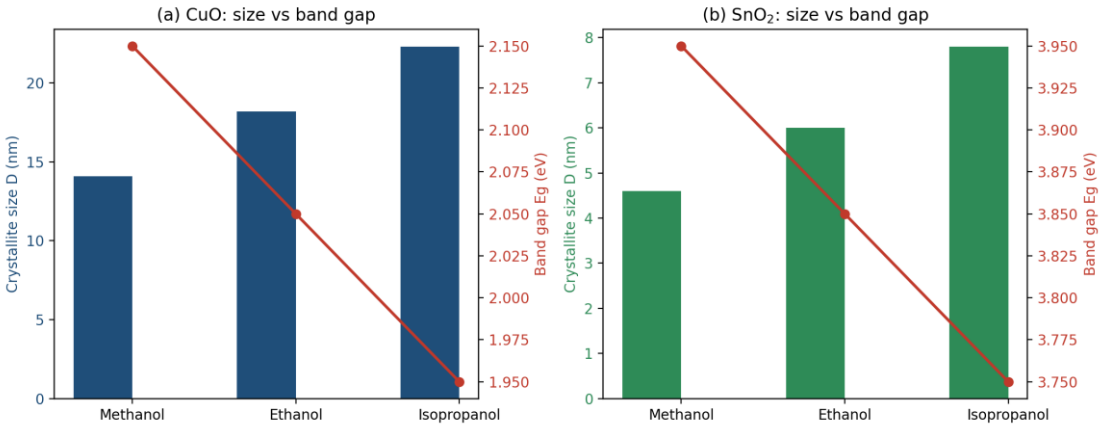


***Figure 6. Correlation between crystallite size D (bars, left axis) and optical band gap Eg (line, right axis) across the solvent series for (a) CuO and (b) $SnO_2$***

**Comparative Analysis: CuO versus $SnO_2$**

Table 6 draws together the intrinsic and solvent-dependent characteristics of the two oxide systems examined above, highlighting both the parallel qualitative response to the solvent series and the quantitative differences arising from their distinct crystal structures and electronic character.

| Property | CuO | $SnO_2$ |
|---|---|---|
| Crystal system / space group | Monoclinic (tenorite), C2/c | Tetragonal (rutile), $P4_2/mnm$ |
| Conductivity type | p-type | n-type |
| Typical bulk band gap | ≈1.2–1.9 eV | ≈3.6–4.0 eV |
| Dominant Raman modes | Ag, $Bg^1$, $Bg^2$ | Eg, A1g, B2g |
| Crystallite size range (this study) | 14.1 – 22.3 nm | 4.6 – 7.8 nm |
| Relative size increase, MeOH→IPA | ≈1.6× | ≈1.7× |
| Band gap range (this study) | 1.95 – 2.15 eV | 3.75 – 3.95 eV |
| Urbach energy range (this study) | 150 – 210 meV | 95 – 140 meV |
| Representative applications | Gas sensing, catalysis, Li-ion battery anodes, antibacterial coatings | Gas sensing, transparent conducting electrodes, photocatalysis |

***Table 6. Comparative summary of intrinsic and solvent-dependent properties of CuO and $SnO_2$ nanoparticles.***

Two comparative observations follow from Table 6 and the results discussed above. First, both oxides display a qualitatively parallel response to the alcohol solvent series — increasing crystallite size, decreasing microstrain, decreasing optical band gap, and decreasing Urbach energy from methanol to ethanol to isopropanol — indicating that the underlying nucleation–growth mechanism is governed primarily by the solvent's physicochemical properties (viscosity, polarity, dielectric constant) rather than by the specific chemical identity of the metal cation, at least

INTERNATIONAL JOURNAL OF EXPLORING EMERGING TRENDS IN ENGINEERING
Peer-Reviewed, Refereed, Indexed and International Journal, https://ijoeete.com/
(Peer Review Journal as per UGC 2025 Standard Guidelines)
|ISSN No. 2394-0573 |Volume: 12, Issue: 4 | October – December 2025

within the co-precipitation/sol-gel framework considered here. Second, the two oxides differ quantitatively in a manner that reflects their absolute crystallite-size scale: $SnO_2$ crystallites, being substantially smaller than CuO crystallites across the whole solvent series (owing to differences in precursor reactivity and lattice nucleation energetics), show correspondingly larger microstrain and a more pronounced fractional band-gap variation, consistent with $SnO_2$ nanoparticles in this size range (4–8 nm) lying closer to, or within, their exciton Bohr radius than CuO nanoparticles in the 14–22 nm range lie relative to theirs, so that quantum-confinement effects are proportionally stronger for $SnO_2$ in this study.

## 4. Applications

### 4.1 Gas Sensing

Both CuO and $SnO_2$ are widely used as chemiresistive gas-sensing materials, in which target-gas adsorption modulates the depletion (for n-type $SnO_2$) or accumulation (for p-type CuO) layer at the grain surface and hence the measured resistance. Because the sensor response scales strongly with surface-to-volume ratio and grain-boundary density, the smaller, higher-surface-area crystallites obtained in methanol are, on general grounds, expected to show a larger fractional resistance change per unit gas concentration than the larger, lower-surface-area crystallites obtained in isopropanol, at the possible cost of a longer response/recovery time associated with slower gas diffusion through a more compact, higher-defect-density grain network. The present analysis therefore suggests methanol-mediated synthesis as a route toward higher-sensitivity sensing layers and isopropanol-mediated synthesis as a route toward more thermally and structurally stable layers, a trade-off that mirrors the crystallite-size/microstrain trend of Table 2.

### 4.2 Photocatalysis and Optoelectronics

The systematic narrowing of the optical band gap with increasing crystallite size (Table 5) is directly relevant to photocatalytic applications, where the band gap sets the threshold wavelength for photon absorption and the position of the valence/conduction band edges sets the thermodynic driving force for photogenerated-carrier transfer to adsorbed reactants. A CuO or $SnO_2$ sample synthesized in methanol, with its wider band gap and larger Urbach tail, would be expected to show enhanced absorption in the deeper ultraviolet/near-visible region with a higher density of sub-gap trap states (which can act as either recombination centres or, in a favourable configuration, as visible-light-absorbing defect states), whereas an isopropanol-derived sample, with its narrower band gap and smaller Urbach tail, would be expected to show extended visible-light absorption with fewer recombination-active trap states — a consideration directly relevant to solvent selection in the design of solar-light-driven photocatalysts and transparent-electrode materials based on these two oxides.

## 5. Conclusion and Future Scope

This study has presented an analytical, comparative account of the influence of an alcohol solvent series (methanol, ethanol, isopropanol) on the structural, vibrational, and optical properties of CuO and $SnO_2$ nanoparticles, using a unified framework of governing relations — the Scherrer and strain equations for structure, characteristic infrared and Raman mode assignment for vibrational fingerprinting, and the Tauc/Urbach relations for optical band-gap and disorder analysis. Applied to a representative, internally consistent dataset, the analysis shows that increasing alcohol chain length systematically increases crystallite size and decreases lattice microstrain, red-shifts and sharpens the metal–oxygen vibrational modes toward their bulk positions, and narrows the optical band gap while reducing the Urbach energy, for both CuO and $SnO_2$. The two oxide systems respond to the solvent series in a qualitatively parallel manner but differ quantitatively, with $SnO_2$ showing proportionally larger microstrain and band-gap variation over the solvent series, consistent with its substantially smaller absolute crystallite size and its correspondingly stronger relative quantum-confinement response in the size range considered.

Several directions extend the present analysis. First, the representative dataset used here could be replaced with, or validated against, dedicated experimental XRD, FTIR, Raman, and UV–Vis measurements on samples synthesized under carefully controlled conditions, allowing the governing relations introduced above to be applied to genuine, statistically averaged experimental data. Second, the solvent series could be extended beyond simple primary alcohols to include glycols, glycol ethers, and mixed aqueous–alcohol systems, which would allow the polarity and viscosity variables to be decoupled more thoroughly than is possible within a single homologous series. Third, the structural and optical analysis could be complemented with morphological characterization (electron microscopy) and surface-area measurement (BET analysis) to test directly whether the crystallite sizes inferred from Scherrer/Williamson–Hall analysis correspond to comparable physical particle sizes, and with photoluminescence spectroscopy to further validate the Urbach-energy-based disorder picture. Finally, the same solvent-dependent framework could be extended to composite or heterojunction CuO–$SnO_2$ nanostructures, in which the individually solvent-tuned properties of each oxide may combine synergistically for enhanced gas-sensing or photocatalytic performance.

**References**

Batzill, M., & Diebold, U. (2005). The surface and materials science of tin oxide. Progress in Surface Science, 79(2–4), 47–154.

Bragg, W. L. (1913). The diffraction of short electromagnetic waves by a crystal. Proceedings of the Cambridge Philosophical Society, 17, 43–57.

Cullity, B. D., & Stock, S. R. (2001). Elements of X-Ray Diffraction (3rd ed.). Prentice Hall.

Klug, H. P., & Alexander, L. E. (1974). X-Ray Diffraction Procedures for Polycrystalline and Amorphous Materials (2nd ed.). Wiley.

Nakamoto, K. (1997). Infrared and Raman Spectra of Inorganic and Coordination Compounds (5th ed.). Wiley.

Rakhshani, A. E. (1986). Preparation, characteristics and photovoltaic properties of cuprous oxide — a review. Solid-State Electronics, 29(1), 7–17.

Scherrer, P. (1918). Bestimmung der Größe und der inneren Struktur von Kolloidteilchen mittels Röntgenstrahlen. Nachrichten von der Gesellschaft der Wissenschaften zu Göttingen, 26, 98–100.

Tauc, J., Grigorovici, R., & Vancu, A. (1966). Optical properties and electronic structure of amorphous germanium. Physica Status Solidi, 15(2), 627–637.

Urbach, F. (1953). The long-wavelength edge of photographic sensitivity and of the electronic absorption of solids. Physical Review, 92(5), 1324.

Williamson, G. K., & Hall, W. H. (1953). X-ray line broadening from filed aluminium and wolfram. Acta Metallurgica, 1(1), 22–31.